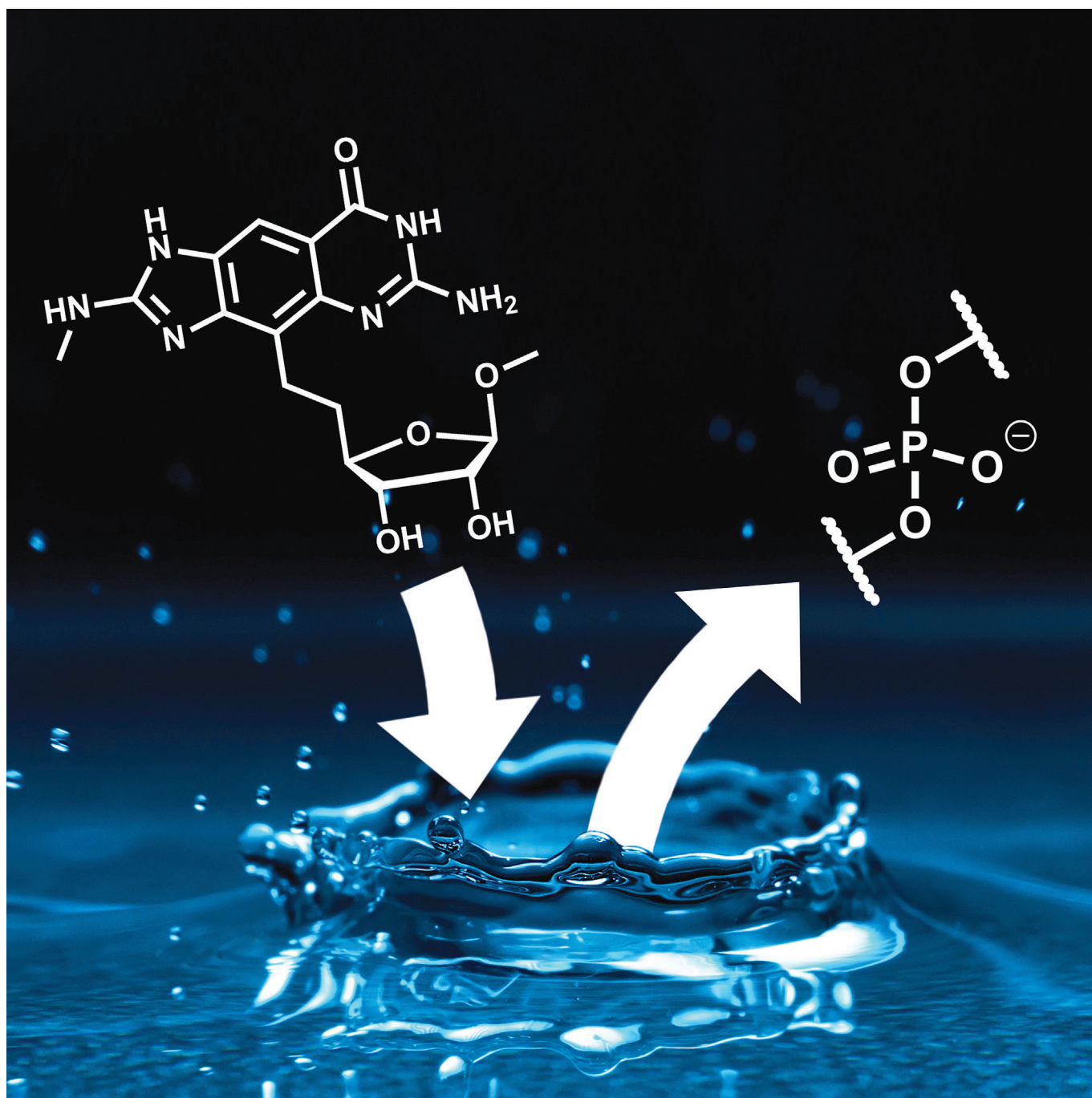


Molecular Recognition | *Hot Paper* Replacement of Water Molecules in a Phosphate Binding Site by Furanoside-Appended *lin*-Benzoguanine Ligands of tRNA-Guanine Transglycosylase (TGT)

Luzi J. Barandun,^[a] Frederik R. Ehrmann,^[b] Daniel Zimmerli,^[c] Florian Immekus,^[b] Maude Giroud,^[a] Claudio Grünenfelder,^[a] W. Bernd Schweizer,^[a] Bruno Bernet,^[a] Michael Betz,^[b] Andreas Heine,^[b] Gerhard Klebe,^{*,[b]} and François Diederich^{*,[a]}

Dedicated to the 20th anniversary of Chemistry—A European Journal



Abstract: The enzyme tRNA-guanine transglycosylase has been identified as a drug target for the foodborne illness shigellosis. A key challenge in structure-based design for this enzyme is the filling of the polar ribose-34 pocket. Herein, we describe a novel series of ligands consisting of furanose-appended *lin*-benzoguanines. They were designed to replace a conserved water cluster and differ by the functional groups at C(2) and C(3) of the furanosyl moiety being either OH or OMe. The unfavorable desolvation of Asp102

and Asp280, which are located close to the ribose-34 pocket, had a significant impact on binding affinity. While the enzyme has tRNA as its natural substrate, X-ray co-crystal structures revealed that the furanosyl moieties of the ligands are not accommodated in the tRNA ribose-34 site, but at the location of the adjacent phosphate group. A remarkable similarity of the position of the oxygen atoms in these two structures suggests furanosides as a potential phosphate isoster.

Introduction

Filling polar binding pockets of an enzyme by a ligand is a difficult task in medicinal chemistry and structure-based drug design.^[1] In particular, phosphate binding sites,^[2] which are present in many classes of enzymes, such as kinases and phosphatases,^[3] are frequently targeted for improving potency and/or selectivity of a drug lead compound. Thereby, the understanding of replacing water molecules in the pocket of the apoenzyme is a key challenge,^[4] and several approaches towards the consideration of water replacement in structure-based drug design and molecular docking have been developed.^[5]

Herein, we present a new approach to the filling of a polar binding pocket in the enzyme tRNA-guanine transglycosylase (TGT; EC 2.4.2.29). It has been shown that TGT is essential in the development of the pathogenicity of *Shigella* bacteria,^[6,7] which cause the severe inflammatory bowel disease shigellosis and over one million lethal cases per year.^[8,9] Bacterial TGT is involved in the modification of tRNA and catalyzes the exchange of guanine by preQ₁ (7-aminomethyl-7-deazaguanine).^[10] Three major pockets are found in the active site of *Zymomonas mobilis* TGT: the central guanine/preQ₁ binding site, where the base-exchange reaction takes place, and the ribose-33 and ribose-34 pockets, where the tRNA backbone is accommodated (Figure 1 a).^[11] We have introduced 2-amino-*lin*-benzoguanines (such as **1**; IUPAC: 6-amino-2-(methylamino)-imidazo[4,5g]quinazolin-8(7*H*)-one) as central ligand scaffold

that binds to the guanine/preQ₁ binding site (Figure 1 b, c).^[12,13] Derivatization at H₂N-C(2) and/or C(4) allowed us to target the ribose-33 pocket,^[14,15] the ribose-34 pocket,^[16,17] or both ribose pockets simultaneously.^[18] Furthermore, we have used ligands based on this scaffold for the modulation of the protein-protein interaction in homo-dimeric TGT,^[19] and studied the thermodynamic profile of ligand binding by isothermal titration calorimetry (ITC).^[20–22]

In the presence of a ligand in the preQ₁/guanine binding site, the uncomplexed polar ribose-34 pocket is solvated by a highly conserved water cluster, which consists of five water molecules (W1–W5; see X-ray crystal structure in Figure 1 c and Supporting Information Figure S1), with water molecule W6 connecting the cluster to the solvent-exposed ribose-33 pocket.^[17] Displacing these water molecules, which solvate the side chains of the aspartates Asp102 and Asp280, by an apolar substituent (compound **2**) led to an unfavorable desolvation of the ribose-34 pocket, which was manifested in the weaker binding affinity ($K_i = 235 \pm 50$ nM) compared to the 4-unsubstituted analogue **1** ($K_i = 58 \pm 36$ nM). Parts of this water cluster were displaced by the polar substituents of ethanol **3** ($K_i = 97 \pm 5$ nM; PDB code: 3E0U^[17]) or protonated amine **4** ($K_i = 55 \pm 3$ nM; PDB code 3GC5^[17]), but without gaining binding affinity. Only by further expanding the substituent into an apolar groove, shaped by Val45, Leu68, and Val282, was it possible to improve the binding affinity (e.g. compound **5**; $K_i = 4 \pm 2$ nM; PDB code: 3EOS^[17]).^[16] These findings were supported by molecular dynamics simulations, which identified nine water binding sites in the ribose-34 pocket, whereby only two of them were found to be favorable for displacement by an apolar ligand.^[23] Although the *lin*-benzoguanine derivatives are very potent ligands, their physicochemical properties are not optimal—in particular their low solubility in both water and organic solvents is a problem for synthesis, biological assays, and potential administration as a drug.^[13] This prompted us to investigate in the current study furanoside-based substituents for the displacement of the water cluster in the ribose-34 pocket (compounds **6 a–c**; Table 1). The hydroxy groups may replace water molecules solvating the polar residues Asp102 and Asp280, but do not introduce an additional charge into the inhibitors, unlike the ethylammonium linker in compounds **4** and **5**. Since the furanosides are not linked by a *N*-glycosidic bond to the *lin*-benzoguanine scaffold, they are expected to be stable towards acidic or enzymatic depurination. Although

[a] Dr. L. J. Barandun,⁺ M. Giroud, C. Grünenfelder, Dr. W. B. Schweizer, Dr. B. Bernet, Prof. Dr. F. Diederich
Laboratorium für Organische Chemie, ETH Zürich
Vladimir-Prelog-Weg 3, HCI, 8093 Zürich (Switzerland)
Fax: (+41)44-632-1109
E-mail: diederich@org.chem.ethz.ch

[b] F. R. Ehrmann,⁺ Dr. F. Immekus, M. Betz, Prof. Dr. A. Heine, Prof. Dr. G. Klebe
Institut für Pharmazeutische Chemie, Philipps-Universität Marburg
Marbacher Weg 6, 35032 Marburg (Germany)
Fax: (+49)6421-282-8994
E-mail: klebe@mail.uni-marburg.de

[c] D. Zimmerli
F. Hoffmann-La Roche Ltd, Discovery Technologies, Bldg 92/5.64C
4070 Basel (Switzerland)

[⁺] These authors contributed equally to this work.

Supporting information for this article is available on the WWW under <http://dx.doi.org/10.1002/chem.201405764>.

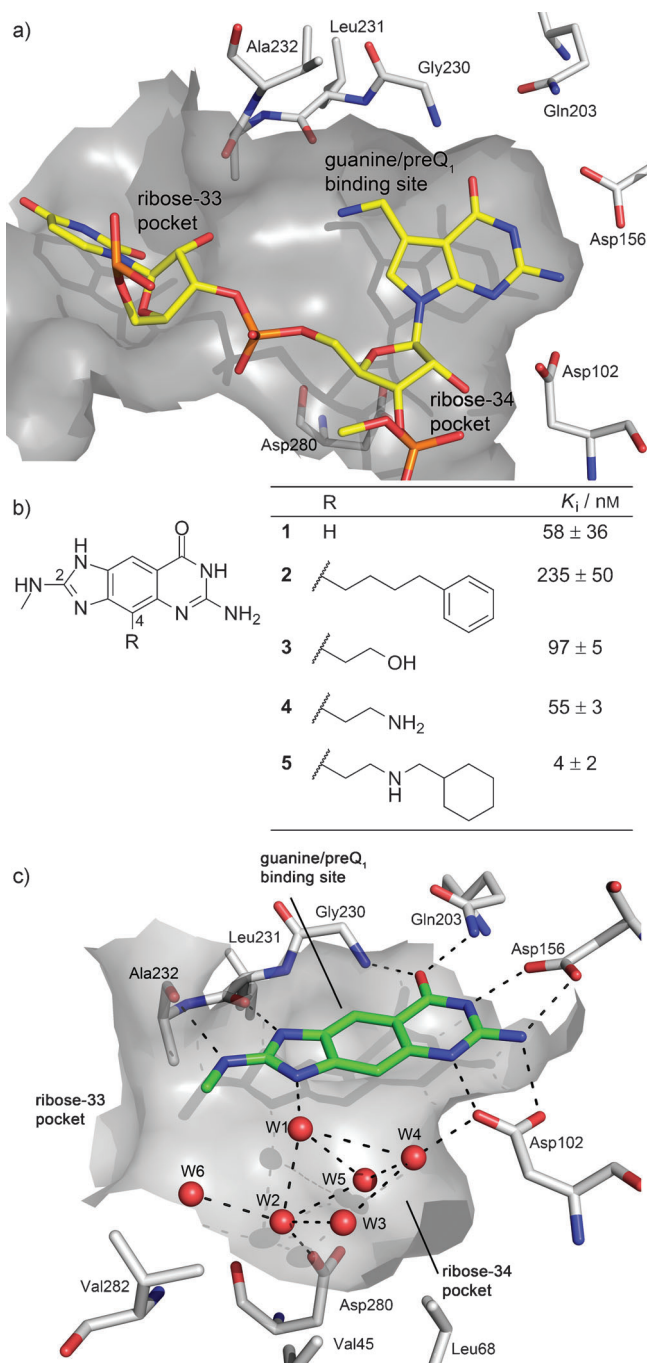


Figure 1. a) Active site of *Z. mobilis* TGT with a preQ₁-tRNA substrate (PDB code: 1Q2S, 3.20 Å resolution^[11]). b) Structure and inhibition constants K_i of **1**,^[14] and **2–5**.^[16] c) X-ray crystal structure of *Z. mobilis* TGT soaked with **1** (1.49 Å resolution, PDB code: 4PUK^[21]). Color code: C_{tRNA} yellow, C_{ligand} green, C_{enzyme} gray, O red, N blue, P orange, enzyme surface gray. Selected water molecules are shown as red spheres and labeled as W. Hydrogen bonds are shown as dashed lines (heavy atom distances between 2.6 and 3.6 Å). These characteristics apply to all figures unless otherwise stated.

several groups have analyzed the role of water molecules in carbohydrate–protein interactions,^[24] furanosides and pyranosides are rarely used in structure-based drug design.

Table 1. Binding affinities, $c\log D_{7,4}$ and $c\log P$ values.

| | R ¹ | R ² | K_i /nM ^[a] | K_d /nM ^[b] | $c\log D_{7,4}$ ^[c] | $c\log P$ ^[d] |
|---------------------|----------------|----------------|--------------------------|--------------------------|--------------------------------|--------------------------|
| β-6a | H | H | 217 ± 81 | 288 ± 55 | −1.5 | −1.3 |
| α/β-6b 15:85 | Me | H | 286 ± 16 | 276 ± 69 | −1.1 | −0.9 |
| β-6c | H | Me | 353 ± 106 | n.d. ^[e] | −1.5 | −1.2 |

[a] Inhibition constant measured by a radioactive assay. K_i values are mean values over at least four measurements. [b] Dissociation constant measured by ITC (see Supporting Information Section S3 for details of the assays). K_d values are mean values over at least five measurements. [c] Logarithmic distribution coefficient for octanol/water at pH 7.4. [d] Logarithmic partition coefficient for octanol/water. Both values were calculated using ACD/Labs software.^[29] [e] Not determined due to shape of curve.

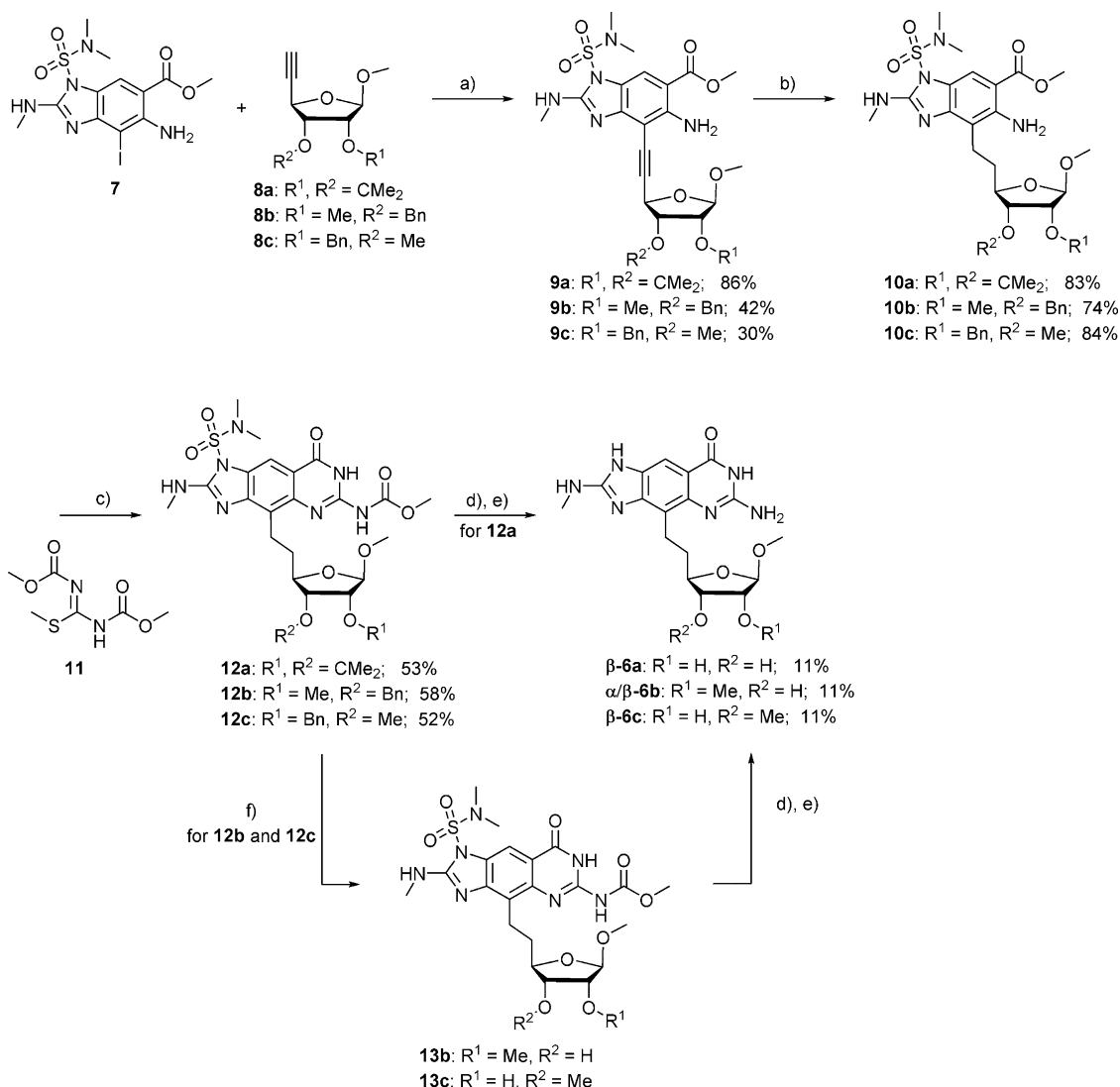
Results and Discussion

Synthesis

Iodobenzimidazole **7** was prepared according to our previously published procedure (Scheme 1).^[14,16] The furanosyl moieties were introduced by Sonogashira cross-coupling reaction of **7** and alkynes **8a–c**. The synthesis of the latter is described in the Supporting Information (Section S2). The resulting alkynated benzimidazoles **9a–c** were obtained in yields of 30–86%. Subsequent hydrogenation of the alkynes to the alkanes **10a–c** (74–84% yield) required a large excess of Raney nickel. Gratifyingly, the benzyl protecting groups were stable under these conditions. Cyclization of the benzimidazoles was achieved by adapting a literature procedure, which used HgCl₂ for the activation of thiourea **11**.^[25] After guanylation, treatment with NaOMe cleaved one methoxycarbonyl group and triggered cyclization to the *lin*-benzoguanines **12a–c** (52–58% yield). Hydrogenation of the benzyl ethers **12b** and **12c** needed a large excess of Pd/C and long reaction times, but afforded quantitatively the corresponding alcohols **13b** and **13c**. The methoxycarbonyl group of **12a**, **13b**, and **13c** was cleaved by hydrolysis with KOH. The removal of the sulfamoyl group required strong acids. Under these conditions, the isopropylidene group of **12a** was cleaved and partial anomerization took place. The resulting α/β -anomers of **6a–c** were separated by HPLC on a chiral stationary phase (Phenomenex Lux 5 μ m Cellulose-2 AXIA packed column) giving pure β -**6a** and β -**6c**, and an enriched sample of α/β -**6b** (15:85).

Conformational analysis

The conformation of the furanose ring of benzimidazole **10b** (Figure 2a) and of 2-*O*-methyl- β -D-ribofuranoside **14** (Figure 2b) in the solid state was determined by X-ray crystallography (for details, see Supporting Information Section S2.5).



Scheme 1. Synthesis and numbering of the furanoside-appended *lin*-benzoguanine ligands for TGT. In contrast to nucleotides, the furanoside has a higher priority in the numbering than the purine moiety. Reagents and conditions: a) [PdCl₂(PPh₃)₂], CuI, DIPA, THF, 50 °C, 4.5–14 h, **9a**: 86%, **9b**: 42%, **9c**: 30%; b) Raney-Ni, H₂, MeOH, 25 °C, 4.5–24 h, **10a**: 83%, **10b**: 74%, **10c**: 84%; c) **11**, HgCl₂, Et₃N, DMF, 50 °C, 3.5–16 h; then NaOMe, MeOH, 50 °C, 1.5–2 h, **12a**: 53%, **12b**: 58%, **12c**: 52%; d) KOH, MeOH, 60 °C, 4–24 h; e) conc. HCl, THF, MeOH, 60 °C, 20–24 h, **β-6a**: 11% (from **12a**), **α/β-6b**: 11% (from **12b**), **β-6c**: 11% (from **12c**); f) Pd/C (10%), H₂, EtOH, 25 °C, 2–4 d. DMF = *N,N*-dimethylformamide, DIPA = *N,N*-diisopropylamine, THF = tetrahydrofuran.

Both furanosides crystallized in a northern conformation, but showed different puckering states according to the Altona–Sundaralingam model.^[26] In **10b**, the *ribo*-hexofuranoside moiety is present in a ¹T₂ twist conformation with a pseudorotational phase *P* of 332° and a puckering amplitude φ_m of 38°. Ribofuranoside **14** shows an E₂ envelope conformation with *P* = 339° and φ_m = 37° (for a schematic overview of the ring puckering, see Figure 2c,d). These conformations are in good agreement with a CSD search by Taha et al. who found a preference for β -ribofuranosides for *P* = 313–360° and φ_m = 34–43°.^[27] The conformations of all furanosides in solution was studied by NMR spectroscopy: the ratio $J_{1,2}/J_{3,4}$ revealed the preference of ring conformations (northern vs. southern conformation)^[26] and the size of $J_{4,5\text{-pro-S}}$ and $J_{4,5\text{-pro-R}}$ evidenced the preferred orientation of the substituent at C(5) (for details, see Supporting Information Section S2.6).^[28] The furanosides β -**6a**–

c adopt in (CD₃)₂SO a northern conformation as evidenced by $J_{1,2} < 1$ Hz. The ethanedyl moiety of β -**6a** and β -**6c** adopts a *gt/tg* equilibrium of ca. 1:1 indicated by $J_{4,5a} = J_{4,5b}$ of about 6.5 Hz. Broad signals prevented the determination of the rotameric equilibrium of α/β -**6b**.

Binding affinities

Compounds **6a–c** are readily water-soluble, which facilitated the assays of their biological activities. The binding affinities of the inhibitors were measured by a radioactive assay, giving K_i , and by ITC, giving K_d (for a description of both assays, see Section S3).^[7,12,20,22] Both assays gave comparable K_i and K_d values in the range of 217–353 nM (Table 1). We recently found for other *lin*-benzoguanine-derived ligands that both K_i and K_d values are in very good agreement, in contrast to the findings

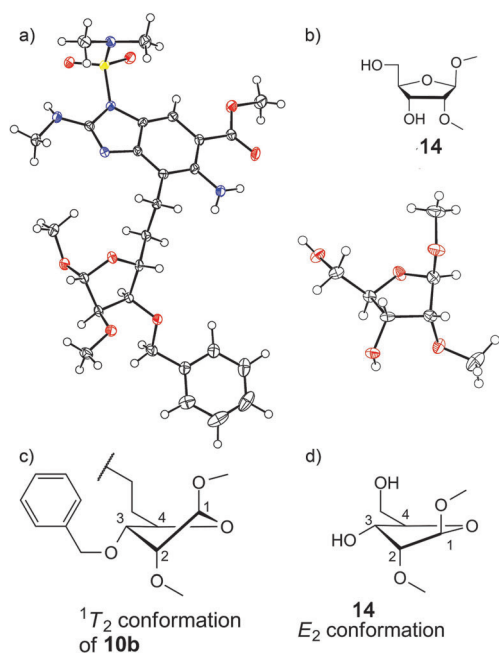


Figure 2. a) ORTEP plot of **10b** (CCDC code: 1016974). b) Structure and ORTEP plot of **14** (CCDC code: 1016992). Schematic representation of the ring pucker of c) **10b** and d) **14**. Atomic displacement parameters obtained at 100 K are shown at the 50% probability level.

for *lin*-benzohypoxanthines, lacking the exocyclic NH₂ group, for which the thermodynamic dissociation constants are much lower than the inhibitory constants (for a detailed discussion, see reference [22]). Compared to ethanol **3** (Figure 1b), the furanoside-based inhibitors have weaker affinities by a factor of about 2–3. While losing some affinity compared to the previous substituted ligands, the ribose derivatives **6a–c** feature the advantage of much enhanced water solubility, which is essential for achieving solubility of the drug in blood. The hydrophilicity of the inhibitors was estimated using ACD/Labs software,^[29] which was shown to predict *clogP* values with a root mean squared error of 0.50 up to 1.28.^[30] Although the predicted values for the *lin*-benzoguanines are close to each other within the error range, a plausible trend is observed comparing their relative hydrophilicities. The ribose derivatives **6a–c** had a reduced hydrophilicity (*clogD_{7.4}* of –1.1 to –1.5) as compared to the protonated ammonium compound derived from **4** (–2.5), but a higher hydrophilicity than the 4-unsubstituted analogue **1** (–0.3) or the cyclohexylmethylammonium derivative from **5** (–0.2). Maintaining a low hydrophilicity of a drug compound is crucial for membrane permeability and, consequently, for its efficacy and good retention in the body.^[31]

X-ray co-crystal structures

For all ligands **β-6a**, **β-6b**, and **β-6c**, highly resolved co-crystal structures with *Z. mobilis* TGT (resolutions 1.17–1.41 Å) were obtained (Table 2).^[32,33] Although a 15:85 anomeric mixture of α/β -**6a** was applied for co-crystallization with *Z. mobilis* TGT,

Table 2. X-ray co-crystal structures: data collection and refinement statistics.

| Crystal data | β-6a | β-6b | β-6c |
|---|-----------------------------|------------------------------|-----------------------------|
| PDB code | 4LEQ | 4LBU | 4KWO |
| A) data collection and processing | | | |
| collection site | BESSY 14.1 | BESSY14.2 | BESSY14.2 |
| No. crystal used | 1 | 1 | 1 |
| λ [Å] | 0.91841 | 0.85507 | 0.91841 |
| space group | C2 | C2 | C2 |
| unit cell parameters | | | |
| <i>a</i> [Å] | 90.6 | 90.3 | 85.2 |
| <i>b</i> [Å] | 65.1 | 65.2 | 65.1 |
| <i>c</i> [Å] | 70.4 | 70.6 | 71.4 |
| β [°] | 96.3 | 96.3 | 94.0 |
| B) diffraction data | | | |
| resolution range [Å] | 50–1.41 (1.43–1.41) | 50–1.17 (1.19–1.17) | 50–1.32 (1.33–1.32) |
| unique reflections | 76331 (3734) ^[a] | 136269 (6654) ^[a] | 90020 (4448) ^[a] |
| <i>R</i> (<i>I</i>) _{sym} [%] | 6.5 (49.7) ^[a] | 4.3 (48.0) ^[a] | 4.1 (43.1) ^[a] |
| completeness [%] | 96.9 (94.7) ^[a] | 99.4 (97.6) ^[a] | 98.3 (96.9) ^[a] |
| redundancy | 3.8 (3.7) ^[a] | 3.1 (2.9) ^[a] | 4.2 (4.0) ^[a] |
| <i>I</i> / σ (<i>I</i>) | 16.6 (2.8) ^[a] | 23.5 (2.1) ^[a] | 28.0 (3.0) ^[a] |
| Matthews coefficient [Å ³ Da ^{−1}] | 2.4 | 2.4 | 2.3 |
| C) refinement | | | |
| program used | Phenix ^[32] | Phenix ^[32] | Phenix ^[32] |
| resolution range [Å] | 40.9–1.41 | 14.9–1.17 | 27.0–1.32 |
| reflins used | 72493 | 129428 | 85496 |
| final <i>R</i> values | | | |
| <i>R</i> _{free} ^[c] | 14.9 (19.7) | 15.2 (22.9) | 16.3 (25.0) |
| <i>R</i> _{work} ^[d] | 12.3 (16.8) | 13.6 (21.8) | 14.6 (19.9) |
| No. of atoms (non-hydrogen) | | | |
| protein atoms | 2984 | 2941 | 2847 |
| water molecules | 428 | 435 | 291 |
| ligand atoms | 28 | 29 | 29 |
| RMSD, angle [°] | 1.1 | 1.1 | 1.1 |
| RMSD, bond [Å] | 0.006 | 0.006 | 0.006 |
| Ramachandran plot ^[e] | | | |
| most favored regions [%] | 94.7 | 93.4 | 95.3 |
| additionally allowed regions [%] | 5.0 | 6.3 | 4.4 |
| generously allowed regions [%] | 0.3 | 0.3 | 0.3 |
| mean B-factors [Å ²] | | | |
| protein atoms | 14.1 | 14.1 | 17.1 |
| water molecules | 30.5 | 30.1 | 30.9 |
| ligand atoms | 11.8 | 13.4 | 15.3 |

[a] Values in parenthesis are statistics for the highest resolution shell. [b] $R(I)_{sym} = [\sum_h \sum_i |I_i(h) - \langle I(h) \rangle| / \sum_h \sum_i I_i(h)] \times 100$, in which $\langle I(h) \rangle$ is the mean of the *I*(*h*) observation of reflection *h*. [c] $R_{work} = \sum_{hkl} |F_o - F_c| / \sum_{hkl} |F_o|$. [d] *R*_{free} was calculated as shown for *R*_{work} but on refinement-excluded 5% of data. [e] Calculated with PROCHECK.^[33]

only the β -anomer was bound suggesting a high preference over the α -anomer. The structures of the enzyme complexes with β -**6a** and β -**6c** are shown in Figure 3a,b, respectively, while the structure with β -**6b** is depicted in Figure S2 in the Supporting Information. In all three structures, the *lin*-benzoguanine core is accommodated in the guanine/preQ₁ binding site forming the same interactions as previously observed for

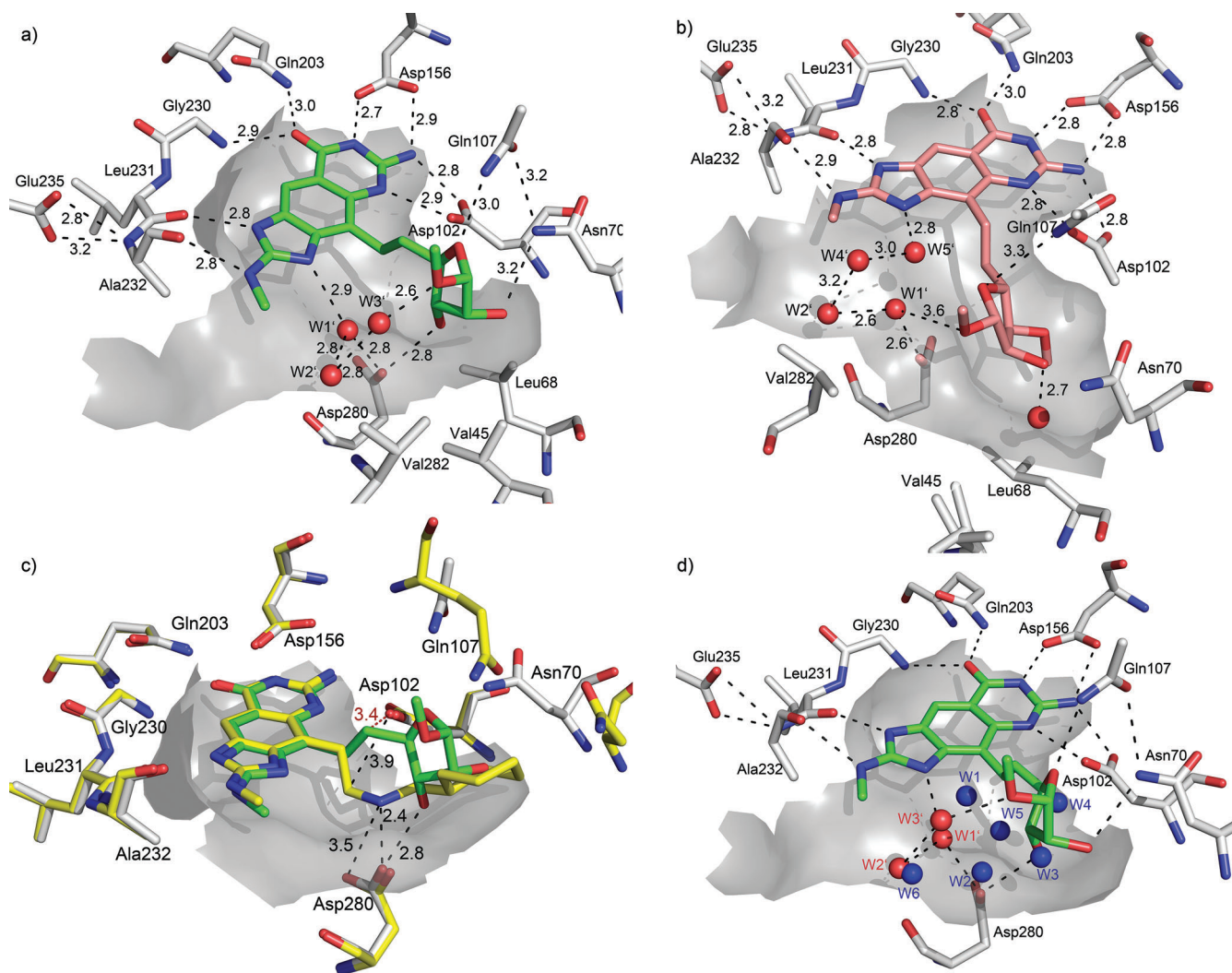


Figure 3. X-ray co-crystal structure of *Z. mobilis* TGT in complex with a) β -6a (C_{ligand} green, 1.41 Å resolution, PDB code: 4 LEQ) and b) β -6c (C_{ligand} salmon, 1.32 Å resolution, PDB code: 4 KWO). c) Positions of the ethanedyl linkers in 5 (C_{ligand} yellow, PDB code: 3EOS^[17]) and β -6a. A close unfavorable contact between the linker and Asp102 is shown as a red dashed line. d) Comparison of the water clusters in the structure with β -6a (W1', W2', and W3', shown as red spheres) and 1 (W1–W6, shown as blue spheres; PDB code: 4PUK^[21]). Distances are given in Å.

1.^[15,17–22] The ligands form an array of hydrogen bonds to the side chains of Asp102, Asp156, and Gln203 and to the peptide backbone of Gly230, Leu231, and Ala232 (Figure 3a,b, Figure S2 in the Supporting Information).

The co-crystal structure with β -6a (PDB code: 4 LEQ, Figure 3a) shows the furanosyl moiety in the ribose-34 pocket in an E_2 envelope conformation with $P=344^\circ$ and $\varphi_m=44^\circ$. It undergoes hydrogen bonding with Asn70, Gln107, and Asp280. Only one hydrogen bond from HO–C(3) of the ribofuranosyl unit is formed to Asp280. From the original five-water cluster (Figure 1d), three water molecules (W3, W4, W5) are displaced by β -6a, two water molecules (W1' and W3'; red) are at a slightly altered position (Figure 3d and Figure S3 in the Supporting Information), and water molecule W2', connecting the cluster to the solvent-exposed ribose-33 pocket, remained at the same position. The methoxy group at C(2) accepts a hydrogen bond from W3'.

The ethanedyl linker, which connects the furanosyl moiety to the *lin*-benzoguanine core of β -6a–c, is oriented away from the bottom of the ribose-34 pocket. This is in contrast to our previous C(4) ethylamino-substituted *lin*-benzoguanines, in which the ethanedyl linker is oriented towards the bottom of the pocket allowing formation of a hydrogen-bond from the ammonium center (compounds 4 and 5) to Asp280 (Figure 3c; PDB code: 3EOS^[17]). In addition, the orientation towards the bottom of the pocket avoids repulsive interactions with Asp102 (e.g. for 5, $d(\text{C}_{\text{ethyl}}\cdots\text{O}_{\text{Asp102}})=3.9$ Å), whereas the orientation towards the top in β -6a brings the ethanedyl linker into unfavorable proximity of Asp102 ($d(\text{C}_{\text{ethyl}}\cdots\text{O}_{\text{Asp102}})=3.4$ Å). Furthermore, this conformation has also an effect on the orientation of side chain of Tyr106 (not shown in Figure 3; see Figure S4), which together with the side chain of Met260 forms a sandwich incorporating the tricyclic *lin*-benzoguanine core. When the ethanedyl linker is oriented towards the top of the pocket, Tyr106 is no longer parallel to the *lin*-benzoguanine

core, but tilted by 50° and undergoes a C–H... π -interaction with the linker.

The superimposition of the crystal structures of TGT in complex with **5** (PDB code: 3EOS^[17]) and β -**6a** shows that the furanosyl moiety does not extend into the hydrophobic patch formed by Val45, Leu68, and Val282 (Figure 3c). The O–C(2) bond of β -**6a**, however, is ideally positioned to direct a lipophilic ether substituent into this patch for additional gain in binding affinity (compare **4** and **5**, Figure 1b).

A similar situation is found for the X-ray co-crystal structure with β -**6b** (Figure S2 in the Supporting Information; PDB code: 4 LBU). The enzyme and the ligand, in particular the furanosyl moiety (E_2 envelope conformation with $P=350^\circ$ and $\varphi_m=44$), adopt a similar geometry to that seen in the structure with β -**6a**. The additional methyl group at O–C(2) points towards the hydrophobic groove of the ribose-34 pocket, consisting of Val45, Leu68, and Val282, confirming the opportunity for filling this pocket with larger, more complementary lipophilic groups and concomitant gain in binding affinity. The positions of the two residual water molecules of the initial cluster also comply to the structure with β -**6a**, although W2' is not observed.

The X-ray co-crystal structure of *Z. mobilis* TGT with β -**6c** (PDB code: 4 KWO, Figure 3b) shows a different orientation and conformation of the furanosyl moiety than β -**6a**. As a result of the additional methyl group at O–C(3), a hydrogen bond to Asp280 is no longer possible. Hence, the furanose ring moves away as compared to the complexes with β -**6a** (Figure 3b) and β -**6b** (Figure S2 in the Supporting Information), avoiding a clash between the highly polar Asp280 side chain and the methoxy group. The furanose ring is no longer in the usual E_2 envelope conformation but in a less stable oT_4 twist conformation with $P=79^\circ$ and $\varphi_m=39^\circ$. In this position, C(1)–O–C(4) forms a hydrogen bond to Gln107. In contrast to the co-crystal structures with β -**6a** and β -**6b**, the ethanediyl linker of β -**6c** is oriented towards the bottom of the pocket. In this position, Tyr106 does not form a C–H... π interaction with the linker, but is oriented parallel to the *lin*-benzoguanine core. Furthermore, the downwards orientation of the ethanediyl group avoids repulsive interactions with Asp102. The water cluster in the co-crystal structure with β -**6c** has an altered pattern and consists of four molecules. Water molecule W2', which corresponds to W6 in the original five-water cluster (Figure 1c) is not displaced by the ligand as in β -**6a** and β -**6b**. The water network comprises W1', which is also seen in the two other co-crystal structures with β -**6a** and β -**6b**, in addition to W4' and W5'.

The structural insights from the three co-crystal structures explain the weaker binding affinity compared to the 4-unsubstituted *lin*-benzoguanine **1** ($K_i=58\pm 36$ nM) and inhibitor **5** ($K_i=4\pm 2$ nM; Figure 1b). In the case of the uncomplexed ribose-34 pocket in the co-crystal structure with **1**, Asp280 is optimally solvated by a water cluster. In the crystal structure in complex with high-affinity ligand **5**, Asp280 interacts with the ammonium center in the linker by forming two charge-assisted hydrogen bonds. In contrast, the furanosyl moieties of β -**6a** and β -**6b** only form one hydrogen bond from HO–C(3) to the anionic Asp280 side chain and reduce the solvation of the

ribose-34 pocket by displacing three water molecules. Ethanol **3** and ammonium derivative **4** are better binders, as they leave a better solvated Asp side chain (c.f. Figure S5 in the Supporting Information). The furanosyl moiety of β -**6c** cannot form a hydrogen bond to the side chain of Asp280 due to the methyl group at O–C(3).

A second negative influence on the binding affinity of the furanosides is the repulsive interaction with Asp102, which comes into unfavorable proximity of the ethanediyl linker of β -**6a** and α/β -**6b**. Inhibitor β -**6c** avoids this penalty, but the furanose moiety has to adopt a ring conformation that is most likely higher in energy.^[27]

Although all three furanosides form additional interactions to the enzyme—such as hydrogen bonds of HO–C(2) to Asn70 and from the cyclic ether O-atom to Gln107—the penalty of desolvation of Asp102 and Asp280 is not compensated.

Phosphate mimic

The natural substrate of TGT is tRNA, the phosphate backbone of which is recognized in the ribose pockets of the enzyme. The overlay of the X-ray crystal structures of *Z. mobilis* TGT in complex with a tRNA substrate and preQ₁ introduced at the wobble position 34 (PDB code: 1Q2S^[11]) and in complex with β -**6a** is shown in Figure 4. The pyrimidone moiety of the *lin*-benzoguanine penetrates deeper into the guanine/preQ₁ binding site than the same moiety of tRNA-bound preQ₁ (about 0.8 Å based on the pyrimidone core). A striking difference is that the complexed tRNA does not form a hydrogen bond to Asp280, which is involved in the catalytic cycle of the enzyme.^[11,34] The ethanediyl linker of the synthetic ligand spans the ribose-34 ring of the tRNA to which preQ₁ is attached. This places the furanosyl moiety of β -**6a** into the position of the phosphate-34 group of the tRNA. For a detailed analysis of the two structures, it must be taken into consideration that the resolution of the X-ray crystal structure with the tRNA substrate is significantly lower (3.20 Å^[11]) compared to the one with β -**6a** (1.41 Å). In addition, the measured atomic distances depend on the overlay of the structures (alignment was based on the amino acid residues in the guanine/preQ₁ binding site). Nevertheless, a qualitative comparison shows that the oxygen atom of the anomeric methoxy group of β -**6a** is at a similar position to O(δ) of the phosphate group of the tRNA ligand ($d[C(1)-O_{\beta-6a}\cdots O(\delta)_{tRNA}] = 1.2$ Å; see Figure 4b for numbering of the atoms). The HO–C(2) moiety of β -**6a** is next to O(γ) ($d[C(2)-O_{\beta-6a}\cdots O(\gamma)_{tRNA}] = 1.6$ Å), while O(α) is located in between of HO–C(2) ($d[C(2)-O_{\beta-6a}\cdots O(\alpha)_{tRNA}] = 1.5$ Å) and HO–C(3) ($d[C(3)-O_{\beta-6a}\cdots O(\alpha)_{tRNA}] = 1.7$ Å). The ether oxygen C(4)–O is near O(β) of the phosphate group ($d[C(4)-O_{\beta-6a}\cdots O(\beta)_{tRNA}] = 1.9$ Å). In addition, the water molecules W1' and W2' in the co-crystal structure with β -**6a** are in proximity of the oxygen atoms of the second phosphate group pointing into the ribose-33 pocket ($d[O_{W1}\cdots O(\gamma')_{tRNA}] = 1.3$ Å and $d[O_{W2}\cdots O(\delta')_{tRNA}] = 0.5$ Å). A similar situation is found for compound β -**6b** (Figure S6a in the Supporting Information). In contrast, no similarity to the phosphate group is apparent for ligand β -**6c** (Figure S6b in the Supporting Information). Given

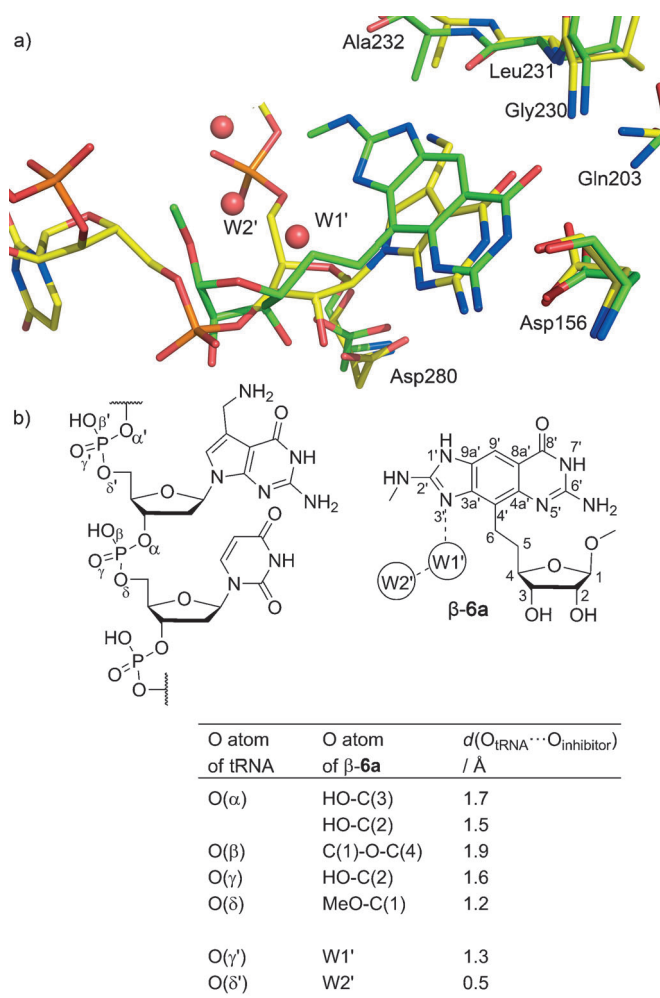


Figure 4. a) Comparison of the X-ray crystal structures of *Z. mobilis* TGT in complex with a preQ₁-tRNA substrate (C yellow, 3.20 Å, PDB code: 1Q2S⁽¹¹⁾) and with β -6a (PDB code: 4 LEQ, C green). b) Comparison of the positions of the oxygen atoms of the phosphate group with the oxygen atoms of furanosyl moiety.

the binding affinities of inhibitors β -6a and β -6b in the nanomolar range, the overlays in Figure 4 and Figure S6a (Supporting Information) suggest that furanosides might be suitable groups to target phosphate binding sites. The filling of these polar pockets is a very challenging task in medicinal chemistry and is often only achieved by charged functional groups that impair membrane permeability.^[35] In this work, we show the potential of furanoside-based ligands to fill the phosphate binding site in *Z. mobilis* TGT. Such substituents have no charge, and the furanosyl moiety increases the water solubility and should not suffer from fast metabolism as it is C–C linked and not C–N linked as in natural nucleotides. Potent neutral phosphate isosters are rare, and this has hampered in particular the development of ligands for the active site of phosphatases; therefore, our future work will focus on validating the hypothesis that furanosides, such as introduced here, have more general phosphate isosteric character.

Conclusion

Herein, we describe a novel series of *lin*-benzoguanines that target the polar ribose-34 pocket of *Z. mobilis* TGT with a furanosyl moiety. The preparation involved a new cyclization strategy for the *lin*-benzoguanine core and the highly challenging separation of the anomeric mixtures by HPLC on a chiral stationary phase. While our previous *lin*-benzoguanine-based inhibitors suffered from poor water solubility, the furanosyl moiety renders **6a–c** freely water soluble. The new compounds had K_i values in the range of 217–353 nM, which makes them weaker inhibitors than ethanol **3** and ethylamine **4** by a factor of 4–6. Based on the analysis of X-ray co-crystal structures, the decrease in binding affinity is due to unfavorable desolvation of Asp102 and Asp280. Although the furanosyl moiety establishes several additional interactions to the enzyme, the removal of three of the five water molecules in the original five-water cluster cannot be compensated. This cluster solvates the ribose-34 pocket in the presence of ligand **1**, which does not penetrate into the pocket. However, the crystal structures also point to the opportunity for regaining binding affinity through extension of the ligands by etherification of HO–C(2) with residues complementary to the hydrophobic patch shaped by Val45, Leu68, and Val282. The comparison of the binding affinities of **4** and **5** shows that much affinity can be gained from proper occupation of this hydrophobic subsite near the ribose-34 pocket. The comparison of the X-ray co-crystal structures in complex with the tRNA-preQ₁ substrate shows an intriguing finding. The furanosyl moiety is not occupying the ribose-34-recognizing area of the enzyme active pocket, but the phosphate-34 binding site. Thereby, the positions of the oxygen atoms of the furanoside resemble the positions of the oxygen atoms in the phosphodiester. This gives rise to the hypothesis that furanosides might be potential surrogates for targeting phosphate binding sites. The further decoration of the furanoside to properly fill the hydrophobic patch and reach the low nanomolar activity range and the validation of furanosides and related sugar derivatives as phosphate isosters are currently pursued in our laboratories.

Experimental Section

All graphics of crystal structures were generated with the program Pymol.^[36] In the following, the experimental details for the syntheses of compounds **6a–c** are described. All other synthetic details and experimental data, conformational analysis of the furanosides, NMR spectra, and description of the radioactive assay, ITC, and crystallization protocols are in the Supporting Information.

General procedure 1 (GP 1) for the cleavage of the methyl carbamates: A solution of the protected aminopyrimidinone (1 equiv) and KOH (10 equiv) in MeOH was stirred at 60 °C for 4–24 h, neutralized (pH \approx 7 \pm 1) by addition of 1 M methanolic HCl solution, and evaporated. The residue was suspended in EtOAc, filtered, and evaporated. The crude product was used in the following step.

General procedure 2 (GP 2) for the cleavage of the *N,N*-dimethylsulfamates: A solution of the protected *lin*-benzoguanine (1 equiv) in THF/MeOH/aq. conc. HCl solution 1:1:1 was stirred at

60 °C for 24 h. Under these conditions, partial anomerization took place. Reaction control was only possible by analytical HPLC ([Nucleosil-100 NH₂, 250×4 mm, 5 μm]; H₂O/MeCN 0:100 for 5 min, 0:100 to 40:60 within 25 min, flow rate 1 mL min⁻¹). The mixture was basified (pH > 7) with a solution of NaOMe in MeOH (20% w/w) and evaporated. The anomers were separated by chiral HPLC ([Phenomenex Lux 5 μm Cellulose-2 Axia packed column, 250×21.2 mm]; heptane/EtOH + 0.01% NH₄OAc 30:70, isocratic for 60 min, flow rate 20 mL min⁻¹). The fractions of the β-D-anomer were further purified by FC (MCI gel; H₂O/MeCN 100:0 to 0:100) or HPLC ([Nucleosil-100 NH₂, 250×21 mm, 5 μm]; H₂O/MeCN 0:100 for 5 min, 0:100 to 30:70 within 25 min, 30:70 for 10 min, flow rate 10 mL min⁻¹). Evaporation and lyophilization gave pure β-D-anomers β-6a and β-6c and an enriched sample of α/β-6b (15:85).

General procedure 3 (GP 3) for the cleavage of the benzyl ethers: A solution of the benzyl ether (1 equiv) in EtOH was treated with 10% Pd/C (200–300% w/w), stirred at 25 °C for 2–4 d under H₂ atmosphere (balloon), centrifuged, and decanted. The residual slurry was suspended in EtOAc, ultrasonicated, centrifuged, and decanted (3×). The combined organic layers were filtered over Celite and evaporated. The crude product was used without further purification in the following step.

Methyl 6-[6-amino-2-(methylamino)-8-oxo-7,8-dihydro-1H-imidazo[4,5g]quinazolin-4-yl]-5,6-dideoxy-β-D-ribo-hexofuranoside (β-6a): According to GP 1, starting from 12a (431 mg, 0.72 mmol) and KOH (403 mg, 7.24 mmol) in MeOH (20 mL). The crude quinoxalinyamine was directly transformed according to GP 2 in THF/MeOH/aq. conc. HCl solution 1:1:1 (9 mL) to an anomeric mixture of α/β-6a. Chiral HPLC ([Phenomenex Lux 5 μm Cellulose-2 AXIA packed column, 250×21.2 mm]; heptane/EtOH + 0.01% NH₄OAc 30:70 isocratic for 60 min, flow rate 20 mL min⁻¹, detected at 264 nm UV), HPLC ([Nucleosil-100 NH₂, 250×21 mm, 5 μm]; H₂O/MeCN 0:100 for 5 min, 0:100 to 30:70 within 25 min, 30:70 for 10 min, flow rate 10 mL min⁻¹; in 5 portions), evaporation, and lyophilization yielded β-6a (30 mg, 11% from 12a) as a white foam. M.p. > 200 °C (decomp); [α]_D²⁵ = -8.5 (c = 0.2 in H₂O); ¹H NMR (600 MHz, (CD₃)₂SO): δ = 1.76–1.87 (m, 2H; H₂C(5)), 2.90 (brs, 3H; NMe), 3.04–3.13 (m, 2H; H₂C(6)), 3.25 (s, 3H; OMe), 3.75 (brq, J ≈ 6.7 Hz, 1H; H-C(4)), 3.76 (d, J = 4.9 Hz, 1H; H-C(2)), 3.92 (dd, J = 6.5, 4.9 Hz, 1H; H-C(3)), 4.61 (s, 1H; H-C(1)), 5.95 (brs, 2H; NH₂), 7.01 (brs, 1H; NH), 7.48 (s, 1H; H-C(9')), 8.30 ppm (brs, 1H; NH); ¹³C NMR (150 MHz, (CD₃)₂SO): δ = 20.88 (Me of AcOH), 21.60 (C(6)), 28.85 (NMe), 35.37 (C(5)), 53.90 (OMe), 74.67 (C(3)), 75.00 (C(2)), 81.74 (C(4)), 103.21 (C(4')), 107.68 (C(1)), 110.06 (C(9')), 117.37 (C(8'a)), 132.64 (C(3'a)), 142.79 (C(9'a)), 145.78 (C(4'a)), 148.86 (C(6')), 158.27 (C(2')), 163.18 (COOH of AcOH), 164.88 ppm (C(8')); IR (ATR): $\tilde{\nu}$ = 3306 (m), 3170 (m), 2937 (m), 2799 (m), 2718 (m), 1697 (m), 1646 (s), 1586 (s), 1525 (m), 1441 (m), 1411 (m), 1376 (m), 1347 (m), 1240 (w), 1198 (w), 1126 (w), 1103 (w), 1087 (w), 1032 (w), 986 (w), 776 (w), 764 (w), 701 cm⁻¹ (w); HR-MALDI-MS: m/z: calcd (%) for C₁₇H₂₃N₆O₅⁺: 391.1724; found: 391.1724 (100) [M + H]⁺.

Methyl 6-[6-amino-2-(methylamino)-8-oxo-7,8-dihydro-1H-imidazo[4,5g]quinazolin-4-yl]-5,6-dideoxy-2-O-methyl-α/β-D-ribo-hexofuranoside (α/β 15:85; α/β-6b): According to GP 3, starting from 12b (130 mg, 0.20 mmol), 10% Pd/C (300 mg), and H₂ (balloon) in EtOH (20 mL). The obtained alcohol 13b was deprotected according to GP 1, using KOH (116 mg, 2.07 mmol) in MeOH (10 mL) to the quinoxalinyamine, which was transformed according to GP 2 in THF/MeOH/aq. conc. HCl solution 1:1:1 (9 mL) to an anomeric mixture of α/β-6b. Chiral HPLC ([Phenomenex Lux 5 μm Cellulose-2 AXIA packed column, 250×21.2 mm]; heptane/EtOH + 0.01% NH₄OAc 30:70 isocratic for 60 min, flow rate 20 mL min⁻¹, detected by 262 nm UV), FC (MCI gel; MeCN/H₂O 0:100 to 100:0), evapora-

tion, and lyophilization yielded α/β-6b 15:85 (9 mg, 11% from 12b) as a white foam. M.p. > 180 °C; ¹H NMR (600 MHz, (CD₃)₂SO; α/β 15:85): signals of β-6b: δ = 1.78–1.82 (m, 2H; H₂C(5)), 2.89 (d, J = 4.9 Hz, 3H; NMe), 3.06–3.16 (m, 2H; H₂C(6)), 3.27 (s, 3H; MeO-C(2)), 3.38 (s, 3H; MeO-C(1)), 3.47 (d, J = 4.3 Hz, 1H; H-C(2)), 3.69–3.75 (m, 1H; H-C(3)), 3.95–4.00 (m, 1H; H-C(4)), 4.73 (brs, 1H; H-C(1)), 5.77–5.85 (brs, 2H; NH₂), 7.00 (brq, J = 4.9 Hz, 1H; NH), 7.47 (s, 1H; H-C(9')), 10.53–10.62 (brs, 1H; NH), 10.87–10.98 ppm (brs, 1H; NH); ¹³C NMR (150 MHz, (CD₃)₂SO; α/β 15:85): signals of β-6b: δ = 21.49 (C(6)), 28.79 (NMe), 35.44 (C(5)), 53.99 (MeO-C(1)), 57.73 (MeO-C(2)), 75.03 (C(3)), 81.90 (C(2)), 84.12 (C(4)), 101.39 (C(4')), 104.78 (C(1)), 109.51 (C(9')), 119.32 (C(8'a)), 130.13 (C(3'a)), 143.61 (C(9'a)), 148.41 (C(6')), 148.71 (C(4'a)), 158.50 (C(2')), 162.76 ppm (C(8')); signals of α-6b: δ = 22.11 (C(6)), 28.89 (NMe), 34.68 (C(5)), 54.13 (MeO-C(1)), 74.26 (C(3)), 82.08 (C(2)), 105.02 (C(4')), 107.46 (C(1)), 111.34 (C(9')), 142.70 (C(9'a)), 157.71 (C(2')), 165.85 ppm (C(8')); IR (ATR): $\tilde{\nu}$ = 3600–2880 (br, w), 2830 (w), 2778 (w), 1690 (w), 1619 (m), 1584 (m), 1520 (m), 1435 (w), 1356 (m), 1186 (w), 1030 (s), 962 (m), 929 (m), 772 cm⁻¹ (m); HR-MALDI-MS: m/z: calcd (%) for C₁₈H₂₅N₆O₅⁺: 405.1881; found: 405.1881 (100) [M + H]⁺.

Methyl 6-[6-amino-2-(methylamino)-8-oxo-7,8-dihydro-1H-imidazo[4,5g]quinazolin-4-yl]-5,6-dideoxy-3-O-methyl-β-D-ribo-hexofuranoside (β-6c): According to GP 3, starting from 12c (190 mg, 0.29 mmol) and 10% Pd/C (400 mg) in EtOH (20 mL). The obtained alcohol 13c was deprotected according to GP 1, using KOH (162 mg, 2.88 mmol) in MeOH (10 mL) to the quinoxalinyamine, which was transformed according to GP 2 in THF/MeOH/aq. conc. HCl solution 1:1:1 (9 mL) to an anomeric mixture of α/β-6c. Chiral HPLC ([Phenomenex Lux 5 μm Cellulose-2 AXIA packed column, 250×21.2 mm]; heptane/EtOH + 0.01% NH₄OAc 30:70 isocratic for 60 min, flow rate 20 mL min⁻¹, detected by 263 nm UV), FC (MCI gel; MeCN/H₂O 0:100 to 100:0), and lyophilization yielded β-6c (15 mg, 11% from 12c) as a white foam. M.p. > 180 °C (decomp); ¹H NMR (600 MHz, (CD₃)₂SO): δ = 1.67–1.76 (m, 1H; H₂-C(5)), 1.82–1.88 (m, 1H; H_b-C(5)), 2.89 (d, J = 4.7 Hz, 3H; NMe), 2.96–3.06 (m, 1H; H_a-C(6)), 3.10–3.20 (m, 1H; H_b-C(6)), 3.30 (s, 3H; MeO-C(3)), 3.32 (s, 3H; MeO-C(1)), 3.59–3.66 (m, 1H; H-C(2)), 3.89 (brq, J ≈ 6.3 Hz, 1H; H-C(4)), 3.97 (brt, J ≈ 4.2 Hz, 1H; H-C(3)), 4.67 (s, 1H; H-C(1)), 4.91 (brs, 1H; HO-C(2)), 5.77 (brs, 2H; NH₂), 6.90 (brs, 1H; NH), 7.46 (s, 1H; H-C(9')), 10.51 (brs, 1H; NH), 10.81 ppm (brs, 1H; NH); ¹³C NMR (150 MHz, (CD₃)₂SO): δ = 21.91 (C(6)), 28.87 (NMe), 35.58 (C(5)), 53.92 (MeO-C(1)), 57.20 (MeO-C(3)), 71.88 (C(2)), 80.48 (C(3)), 84.49 (C(4)), 101.17 (C(4')), 108.16 (C(1)), 109.30 (C(9')), 119.77 (C(3'a)), 130.36 (C(8'a)), 143.40 (C(9'a)), 148.24 (C(6')), 149.07 (C(4'a)), 158.53 (C(2')), 162.81 ppm (C(8')); IR (ATR): $\tilde{\nu}$ = 3630–2649 (w), 1702 (m), 1587 (s), 1540 (s), 1439 (m), 1344 (m), 1180 (m), 1073 (s), 982 (m), 790 (w), 757 cm⁻¹ (w); HR-MALDI-MS: m/z: calcd (%) for C₁₈H₂₅N₆O₅⁺: 405.1881; found: 405.1880 (100) [M + H]⁺.

Acknowledgements

This work was supported by the ETH Research Council and by F. Hoffmann-La Roche, Basel. We acknowledge the beamline support of Bessy II in Berlin for practical help and the HZB for travel grants. We thank Dr. Nils Trapp for help with the small molecule crystal structures and Oliver Dumele for DFT calculations.

Keywords: molecular recognition · phosphate binding sites · shigellosis · structure-based design · water cluster

- [1] C. Bissantz, B. Kuhn, M. Stahl, *J. Med. Chem.* **2010**, *53*, 5061–5084.
- [2] For a general overview of molecular recognition of phosphate groups, see: A. K. H. Hirsch, F. R. Fischer, F. Diederich, *Angew. Chem. Int. Ed.* **2007**, *46*, 338–352; *Angew. Chem.* **2007**, *119*, 342–357.
- [3] T. Hunter, *Cell* **1995**, *80*, 225–236.
- [4] a) F. A. Quijcho, D. K. Wilson, N. C. Vyas, *Nature* **1989**, *340*, 404–407; b) J. D. Dunitz, *Science* **1994**, *264*, 670; c) J. E. Ladbury, *Chem. Biol.* **1996**, *3*, 973–980; d) C. Barillari, J. Taylor, R. Viner, J. W. Essex, *J. Am. Chem. Soc.* **2007**, *129*, 2577–2587; e) P. Ball, *Chem. Rev.* **2008**, *108*, 74–108; f) J. Michel, J. Tirado-Rives, W. L. Jorgensen, *J. Am. Chem. Soc.* **2009**, *131*, 15403–15411; g) M. Ellermann, R. Jakob-Roetne, C. Lerner, E. Borroni, D. Schlatter, D. Roth, A. Ehler, M. G. Rudolph, F. Diederich, *Angew. Chem. Int. Ed.* **2009**, *48*, 9092–9096; *Angew. Chem.* **2009**, *121*, 9256–9260; h) B. Breiten, M. R. Lockett, W. Sherman, S. Fujita, M. Al-Sayah, H. Lange, C. M. Bowers, A. Heroux, G. Krilov, G. M. Whitesides, *J. Am. Chem. Soc.* **2013**, *135*, 15579–15584; i) S. G. Krimmer, M. Betz, A. Heine, G. Klebe, *ChemMedChem* **2014**, *9*, 833–846.
- [5] a) A. T. Garcia-Sosa, R. L. Mancera, P. M. Dean, *J. Mol. Model.* **2003**, *9*, 172–182; b) M. L. Verdonk, G. Chessari, J. C. Cole, M. J. Hartshorn, C. W. Murray, J. W. M. Nissink, R. D. Taylor, R. Taylor, *J. Med. Chem.* **2005**, *48*, 6504–6515; c) B. C. Roberts, R. L. Mancera, *J. Chem. Inf. Model.* **2008**, *48*, 397–408; d) A. Amadasi, J. A. Surface, F. Spyrikis, P. Cozzini, A. Mozzarelli, G. E. Kellogg, *J. Med. Chem.* **2008**, *51*, 1063–1067; e) T. Beuming, R. Farid, W. Sherman, *Protein Sci.* **2009**, *18*, 1609–1619; f) S. B. A. de Beer, N. P. E. Vermeulen, C. Oostenbrink, *Curr. Top. Med. Chem.* **2010**, *10*, 55–66; g) D. D. Robinson, W. Sherman, R. Farid, *ChemMedChem* **2010**, *5*, 618–627; h) L. Wang, B. J. Berne, R. A. Friesner, *Proc. Natl. Acad. Sci. USA* **2011**, *108*, 1326–1330.
- [6] J. M. Durand, N. Okada, T. Tobe, M. Watarai, I. Fukuda, T. Suzuki, N. Nakata, K. Komatsu, M. Yoshikawa, C. Sasakawa, *J. Bacteriol.* **1994**, *176*, 4627–4634.
- [7] U. Grädler, H.-D. Gerber, D. M. Goodenough-Lashua, G. A. Garcia, R. Ficner, K. Reuter, M. T. Stubbs, G. Klebe, *J. Mol. Biol.* **2001**, *306*, 455–467.
- [8] For an overview of *Shigella*, see: a) P. J. Sansonetti, *FEMS Microbiol. Rev.* **2001**, *25*, 3–14; b) S. K. Niyogi, *J. Microbiol.* **2005**, *43*, 133–143; c) B. S. Marteyn, A. D. Gazi, P. J. Sansonetti, *Gut. Microbes* **2012**, *3*, 104–120.
- [9] a) K. L. Kotloff, J. P. Winickoff, B. Ivanoff, J. D. Clemens, D. L. Swerdlow, P. J. Sansonetti, G. K. Adak, M. M. Levine, *WHO Bull.* **1999**, *77*, 651–666; b) P. J. Sansonetti, *PLoS Med.* **2006**, *3*, e354.
- [10] a) D. Iwata-Reuyl, *Bioorg. Chem.* **2003**, *31*, 24–43; b) R. M. McCarty, V. Bandarian, *Bioorg. Chem.* **2012**, *43*, 15–25.
- [11] W. Xie, X. Liu, R. H. Huang, *Nat. Struct. Biol.* **2003**, *10*, 781–788.
- [12] E. A. Meyer, N. Donati, M. Guillot, W. B. Schweizer, F. Diederich, B. Stengl, R. Brenk, K. Reuter, G. Klebe, *Helv. Chim. Acta* **2006**, *89*, 573–597.
- [13] L. J. Barandun, F. Immekus, P. C. Kohler, S. Tonazzi, B. Wagner, S. Wendelspiess, T. Ritschel, A. Heine, M. Kansy, G. Klebe, F. Diederich, *Chem. Eur. J.* **2012**, *18*, 9246–9257.
- [14] S. R. Hörtner, T. Ritschel, B. Stengl, C. Kramer, W. B. Schweizer, B. Wagner, M. Kansy, G. Klebe, F. Diederich, *Angew. Chem. Int. Ed.* **2007**, *46*, 8266–8269; *Angew. Chem.* **2007**, *119*, 8414–8417.
- [15] T. Ritschel, S. Hoertner, A. Heine, F. Diederich, G. Klebe, *ChemBioChem* **2009**, *10*, 716–727.
- [16] P. C. Kohler, T. Ritschel, W. B. Schweizer, G. Klebe, F. Diederich, *Chem. Eur. J.* **2009**, *15*, 10809–10817.
- [17] T. Ritschel, P. C. Kohler, G. Neudert, A. Heine, F. Diederich, G. Klebe, *ChemMedChem* **2009**, *4*, 2012–2023.
- [18] L. J. Barandun, F. Immekus, P. C. Kohler, T. Ritschel, A. Heine, P. Orlando, G. Klebe, F. Diederich, *Acta Crystallogr. Sect. D* **2013**, *69*, 1798–1807.
- [19] a) T. Ritschel, C. Atmanene, K. Reuter, A. Van Dorsselaer, S. Sanglier-Cianferani, G. Klebe, *J. Mol. Biol.* **2009**, *393*, 833–847; b) F. Immekus, L. J. Barandun, M. Betz, F. Debaene, S. Petiot, S. Sanglier-Cianferani, K. Reuter, F. Diederich, G. Klebe, *ACS Chem. Biol.* **2013**, *8*, 1163–1178.
- [20] S. Grüner, M. Neeb, L. J. Barandun, F. Sielaff, C. Hohn, S. Kojima, T. Steinmetz, F. Diederich, G. Klebe, *Biochim. Biophys. Acta* **2014**, *1840*, 2843–2850.
- [21] M. Neeb, P. Czodrowski, A. Heine, L. J. Barandun, C. Hohn, F. Diederich, G. Klebe, *J. Med. Chem.* **2014**, *57*, 5554–5565.
- [22] M. Neeb, M. Betz, A. Heine, L. J. Barandun, C. Hohn, F. Diederich, G. Klebe, *J. Med. Chem.* **2014**, *57*, 5566–5578.
- [23] S. Riniker, L. J. Barandun, F. Diederich, O. Krämer, A. Steffen, W. F. van Gunsteren, *J. Comput.-Aided Mol. Des.* **2012**, *26*, 1293–1309.
- [24] a) W. E. Minke, D. J. Diller, W. G. J. Hol, C. L. M. J. Verlinde, *J. Med. Chem.* **1999**, *42*, 1778–1788; b) C. Clarke, R. J. Woods, J. Gluska, A. Cooper, M. A. Nutley, G.-J. Boons, *J. Am. Chem. Soc.* **2001**, *123*, 12238–12247; c) S. M. Tschampel, R. J. Woods, *J. Phys. Chem. A* **2003**, *107*, 9175–9181; d) A. H. Daranas, H. Shimizu, S. W. Homans, *J. Am. Chem. Soc.* **2004**, *126*, 11870–11876; e) Z. Li, T. Lazaridis, *J. Phys. Chem. B* **2005**, *109*, 662–670; f) K. Saraboji, M. Håkansson, S. Genheden, C. Diehl, J. Qvist, U. Weiningner, U. J. Nilsson, H. Leffler, U. Ryde, M. Akke, D. T. Logan, *Biochemistry* **2012**, *51*, 296–306.
- [25] P. E. Morris, Jr., A. J. Elliott, J. A. Montgomery, *J. Heterocycl. Chem.* **1999**, *36*, 423–427.
- [26] C. Altona, M. Sundaralingam, *J. Am. Chem. Soc.* **1972**, *94*, 8205–8212.
- [27] H. A. Taha, M. R. Richards, T. L. Lowary, *Chem. Rev.* **2013**, *113*, 1851–1876.
- [28] A. Ritter, D. Egli, B. Bernet, A. Vasella, *Helv. Chim. Acta* **2008**, *91*, 673–714.
- [29] ACD/Labs, Version 12.01, I. Advanced Chemistry Development, Toronto, **2009**.
- [30] R. Mannhold, G. I. Poda, C. Ostermann, I. V. Tetko, *J. Pharm. Sci.* **2009**, *98*, 861–893.
- [31] H. Van de Waterbeemd, H. Lennernas, P. Artursson, *Drug Bioavailability: Estimation of Solubility, Permeability, Absorption and Bioavailability*, Wiley-VCH, Weinheim, **2003**.
- [32] P. D. Adams, P. V. Afonine, G. Bunkóczi, V. B. Chen, I. W. Davis, N. Echols, J. J. Headd, L.-W. Hung, G. J. Kapral, R. W. Grosse-Kunstleve, A. J. McCoy, N. W. Moriarty, R. Oeffner, R. J. Read, D. C. Richardson, J. S. Richardson, T. C. Terwilliger, P. H. Zwart, *Acta Crystallogr. Sect. D* **2010**, *66*, 213–221.
- [33] R. A. Laskowski, M. W. MacArthur, D. S. Moss, J. M. Thornton, *J. Appl. Crystallogr.* **1993**, *26*, 283–291.
- [34] D. M. Goodenough-Lashua, G. A. Garcia, *Bioorg. Chem.* **2003**, *31*, 331–344.
- [35] a) C. S. Rye, J. B. Baell, *Curr. Med. Chem.* **2005**, *12*, 3127–3141; b) N. A. Meanwell, *J. Med. Chem.* **2011**, *54*, 2529–2591; c) T. S. Elliott, A. Slowey, Y. Ye, S. J. Conway, *MedChemComm* **2012**, *3*, 735–751.
- [36] The PyMOL Molecular Graphics System, Version 1.6.0.0; Schrödinger, LLC., **2012**.

Received: October 21, 2014
Published online on December 5, 2014